The in vitro therapeutic activity of betulinic acid nanocomposite on breast cancer cells (MCF-7) and normal fibroblast cell (3T3)

ARTICLE *in* JOURNAL OF MATERIALS SCIENCE · DECEMBER 2014

Impact Factor: 2.37 · DOI: 10.1007/s10853-014-8526-3

4 AUTHORS:

Samer Hasan Hussein Al Ali
Faculty of Pharmacy-Isra University, Jordan
36 PUBLICATIONS **309** CITATIONS
SEE PROFILE

Palanisamy Arulselvan
Putra University, Malaysia
66 PUBLICATIONS **549** CITATIONS
SEE PROFILE

Sharida Fakurazi
Putra University, Malaysia
124 PUBLICATIONS **627** CITATIONS
SEE PROFILE

Mohd Zobir Hussein
Putra University, Malaysia
277 PUBLICATIONS **2,788** CITATIONS
SEE PROFILE

J Mater Sci (2014) 49:8171–8182
DOI 10.1007/s10853-014-8526-3

The in vitro therapeutic activity of betulinic acid nanocomposite on breast cancer cells (MCF-7) and normal fibroblast cell (3T3)

Samer Hasan Hussein-Al-Ali · Palanisamy Arulselvan · Sharida Fakurazi · Mohd Zobir Hussein

Received: 21 March 2014 / Accepted: 22 July 2014 / Published online: 13 August 2014

Abstract In the present study, magnetic nanoparticles (MNPs) were coated with chitosan (CS) polymer to form CS–MNP nanoparticles. The CS–MNP were loaded with an anticancer drug, betulinic acid (BA) to form a BA–CS–MNP nanocomposite. The prepared nanocomposite was characterized using XRD, FTIR, TGA, VSM, SEM, TEM, and zeta potential techniques. The release behavior of the BA from the nanocomposite was investigated at pH 7.4, and the study found that the release of BA followed a pseudo-second-order kinetic model. The potential cytotoxicity of free BA, MNPs, CS–MNP, and the BA–CS–MNP nanocomposite was evaluated using normal mouse fibroblast cells (3T3) and breast cancer cells (MCF-7). BA and the nanocomposite at concentrations in the range 0.781–50 μg mL^{-1} did not affect the viability of normal cells during 72 h of incubation. The BA and BA–CS–MNP nanocomposite exhibited cytotoxicity in MCF-7 cells in a dose-dependent manner with IC_{50} values of 2 and 3.6 μg mL^{-1}, respectively.

S. H. Hussein-Al-Ali
Laboratory of Molecular Biomedicine, Institute of Bioscience, Universiti Putra Malaysia, Serdang, Malaysia
e-mail: sameralali72@yahoo.com

S. H. Hussein-Al-Ali
Faculty of Pharmacy, Isra University, P.O. Box 22, Amman 11622, Jordan

P. Arulselvan · S. Fakurazi
Laboratory of Vaccines and Immunotherapeutics, Institute of Bioscience, Universiti Putra Malaysia, Serdang, Malaysia
e-mail: arulbio@gmail.com

S. Fakurazi
e-mail: sharida@upm.edu.my

S. Fakurazi
Department of Human Anatomy, Faculty of Medicine and Health Sciences, Universiti Putra Malaysia, Serdang, Malaysia

M. Z. Hussein (✉)
Materials Synthesis and Characterization Laboratory, Institute of Advanced Technology (ITMA), Universiti Putra Malaysia, Serdang, Malaysia
e-mail: mzobir@upm.edu.my

Introduction

Betulinic acid [(3β)-3-hydroxy-lup-20(29)-en-28-oic acid] is a natural product, a pentacyclic lupane-type triterpene. BA has antiretroviral, antimalarial, and anti-inflammatory properties. In addition, BA shows inhibition properties against cancers such as human melanoma [1], brain tumors [2, 3], ovarian carcinoma [2], human leukemia HL-60 cells [4], and malignant head and neck squamous cell carcinoma SCC25 and SCC9 cell lines [5].

The main impediment to clinical use of BA lies in its poor solubility in aqueous media such as blood serum and polar solvents used for bioassays, which affects the biological activity. To avoid the problem of hydrosolubility and to develop the pharmacological properties, different derivatives were synthesized and evaluated for cytotoxic activity. These derivatives decreased the cytotoxic properties of BA. For example, Kim developed C-20 modified BA, and the data show that the derivative lost the cytotoxicity of BA [6]. Another derivative of BA is prepared by the hydroxylation of C-7 and C-15, and the result shows the loss of BA activity [7]. Different research groups have applied the BA to different human cancer cells such as colon, squamous, breast, prostate, Walker 256 murine carcinosarcoma, and L1210 murine lymphocytic leukemia [1], and they found that the BA had no effect on those cells.

Nanotechnology has developed to such an extent that it is possible to increase the activity of drugs toward cancer

cells. For example, magnetic nanoparticles (MNPs) loaded with arginine or with paclitaxel and rapamycin increased the anticancer properties of these drugs against breast adenocarcinoma cells (MCF-7) [8, 9]. The antitumor activity of 10-hydroxycamptothecin-MNPs against HepG2 cells was increased significantly in comparison with the free 10-hydroxycamptothecin [10].

In recent years, MNPs have received considerable attention because of their versatile features such as superparamagnetism [11], lack of toxicity [12], good biocompatibility, potential for targeted delivery [13, 14], low production cost, hyperthermia [15–17], magnetic resonance imaging [14], and controlled drug release. These properties allow the potential use of MNPs in various nanotechnology applications.

From the literature, MNPs was coated with different polymers for example chitosan. This polymer is the second most abundant polymer in nature and derived from chitin [18]. It is of a major importance in medicine due to special properties, such as biodegradable and biocompatible, and has many reactive functional groups that can serve as an anchor in therapeutics science and binding of many agents [18, 19].

In this work, our purpose is to load the BA on the surface of the CS–MNP nanoparticle to form the BA–CS–MNP nanocomposite and study the drug loading and release profile from final product. X-ray diffraction (XRD), transmission electron microscope (TEM), thermogravimetric analysis (TGA), Fourier transform infrared spectroscopy (FTIR), and vibrating sample magnetometer (VSM) were used to characterize the synthesized nanocomposite. The novelty of this work is the study of the cytotoxicity of the final nanocomposite and comparison of the anticancer properties of BA in the nanocomposite with free BA.

Materials and methods

Materials

Iron(II) chloride tetrahydride ($FeCl_2{\cdot}4H_2O$), iron(III) chloride hexahydrate ($FeCl_3{\cdot}6H_2O$), acetic acid (CH_3-COOH), and sodium hydroxide (NaOH) were obtained from Merck, Germany; chitosan (LMW, 85 % deacetylated) was purchased from Sigma-Aldrich Chemie GmbH, Germany. Deionized water was used for all the experiments. Dimethyl sulfoxide (DMSO) was purchased from Ajax Finechem (Sydney, Australia) with 0.1 % water content and used as the solvent.

Preparation of iron oxide nanoparticles (MNPs)

For preparation of MNPs, the solutions of Fe ions were prepared from iron(II) chloride tetrahydrate ($FeCl_2{\cdot}4H_2O$) and iron(III) chloride hexahydrate ($FeCl_3{\cdot}6H_2O$) salts. The coprecipitation of Fe(II) and Fe(III) salts at a 1:2 ratio takes place using a solution of 2 M NaOH [20]. The precipitates of MNPs were produced according to the reaction given below:

$$2FeCl_3 + FeCl_2 + 8NaOH \rightarrow Fe_3O_4 + 8NaCl + 4H_2O$$

The solution was sonicated for 60 min at room temperature. The black precipitate was ultimately collected by centrifuge separation and was separately washed three times with deionized water.

Preparation of the CS–MNP nanoparticles

The CS solution was prepared by dissolving 0.5 g of CS powder in a 1 % acetic acid solution with stirring for 30 min. CS–MNP nanoparticles were prepared by mixing CS solution with a suspension of Fe_3O_4 nanoparticles [21]. After the mixture was stirred for 18 h and mixed completely, the coated particles were separated by a permanent magnet and were dried at 70 °C for 2 h. The product was denoted as CS–MNP (chitosan–coated MNPs).

Preparation of the BA–CS–MNP nanocomposite

The solution of BA was prepared by dissolving BA into DMSO. The BA–CS–MNP nanocomposite was prepared by mixing a solution of BA (5 mg mL^{-1}) with a known weight of CS–MNP nanoparticles (40 mg mL^{-1}). The solution was magnetically stirred at room temperature for 18 h to facilitate BA uptake. The product was separated by the use of a permanent magnet and was denoted as BA–CS–MNP (loaded BA on the chitosan–coated MNPs).

BA quantities loaded and released from BA–CS–MNP nanocomposite

To measure the amount of BA loaded in the BA–CS–MNP nanocomposite, 5 mg of the nanocomposite was weighed and dissolved in a concentrated mixture of HCl with HNO_3. This set of conditions completely dissolved this nanocomposite and released 100 % of the BA content. Next, the amount of BA loaded was measured using ultraviolet–visible spectroscopy using BA absorbance at 208 nm and a calibration curve.

BA release profiles from the nanocomposite were determined at room temperature using a phosphate-buffered saline (PBS) solution at a concentration of 0.01 mol L^{-1} at pH 7.4. Approximately 85 mg of the nanocomposite was added to 500 mL of the PBS medium. The cumulative amount of BA released into the solution was measured at preset time intervals at $\lambda_{max} = 208$ nm using a Perkin–Elmer UV–Vis spectrophotometer, model Lambda 35.

To compare the release rate of BA from the BA–CS–MNP nanocomposite with the physical mixture, which contained BA with CS and MNPs, 3.0 mg of the physical mixture was obtained by mixing 0.2 mg of BA with 0.05 mg of CS and 2.75 mg of MNP nanoparticles. The release of the active BA was determined as described above.

Cell culturing and MTT cytotoxicity assays

Normal mouse fibroblast cells (3T3) and breast cancer cells were obtained from the American Type Culture Collection (ATCC, Manassas, VA, USA). The cells were maintained and cultured in DMEM medium with 10 % fetal bovine serum (FBS), 15 mmol L^{-1} L-glutamine, 100 units mL^{-1} penicillin, and 100 μg mL^{-1} streptomycin to maintain cells at 37 °C and 5 % CO_2 in a humidified incubator. Media were changed every 2 days, and at 90 %, confluent cells were seeded into a 96-well plate at 1×10^5 cells mL^{-1} and kept overnight for cell attachment. The old media were discarded, and 100 μL of the new medium containing pure BA, CS–MNP, MNPs, and BA–CS–MNP was used to treat the cells, while wells containing media and cells were only used as controls. For each experiment, freshly prepared stock solutions of BA, CS–MNP, MNPs, and BA–CS–MNP were used for the treatment. A stock of 10 mg mL^{-1} (in PBS) was made. Using DMEM, the desired concentrations of the media needed for the treatment were made through serial dilution (0–100 μg mL^{-1}). The MTT assay was used 72 h post-exposure to determine the toxic effect of these agents.

In the MTT assay, the treatment media were discarded after 72 h and MTT-containing media were added at 5 mg mL^{-1} PBS and a volume of 100 μL per well, and the plates were incubated at 37 °C in a 5 % CO_2 humidified incubator. Two hours later, a detergent reagent (DMSO) was then added to the cells to stop the conversion and solubilize the formazan. The amount of formazan correlates directly with the number of viable cells after treatment. Absorbance of the formazan that is formed is taken at a wavelength of 570 nm using a multiwall microplate reader. The experiment was performed in triplicate, and the result was expressed as the mean ± SD.

$$\text{Cell viability } (\%) = \text{Average of treated/average control} \times 100\%$$

Instrumentation

Powder X-ray diffraction (XRD) patterns were used to determine the crystal structure of the samples in the range of 25°–70° on an XRD-6000 diffractometer (Shimadzu, Tokyo, Japan) using CuK_α radiation ($\lambda = 1.5406$ Å) at 30 kV and 30 mA. Fourier transform infrared spectroscopy (FTIR) spectra of the materials were recorded over the range of 400–4000 cm^{-1} on a Thermo Nicolet Nexus, Smart Orbit spectrometer using the KBr disk method. Thermogravimetric analysis was carried out using a Metter-Toledo 851e instrument (Switzerland) with a heating rate of 10 °C min^{-1}, in 150-μL alumina crucibles and in the range of 30–900 °C. Magnetic properties were evaluated by a Lake Shore 7404 vibrating sample magnetometer (VSM). The zeta potential was measured at 25 °C by dynamic light scattering (DLS) using a Malvern Zetasizer Nano ZS (Malvern Instruments, Malvern, UK). The mean particle size of the samples was obtained using a transmission electron microscope (TEM) (Hitachi H-7100, Tokyo, Japan) with an accelerating voltage of 80 and 200 kV. UV–Vis spectra were measured to determine the optical properties in a controlled release study, using an ultraviolet–visible spectrophotometer (Perkin–Elmer, Waltham, MA).

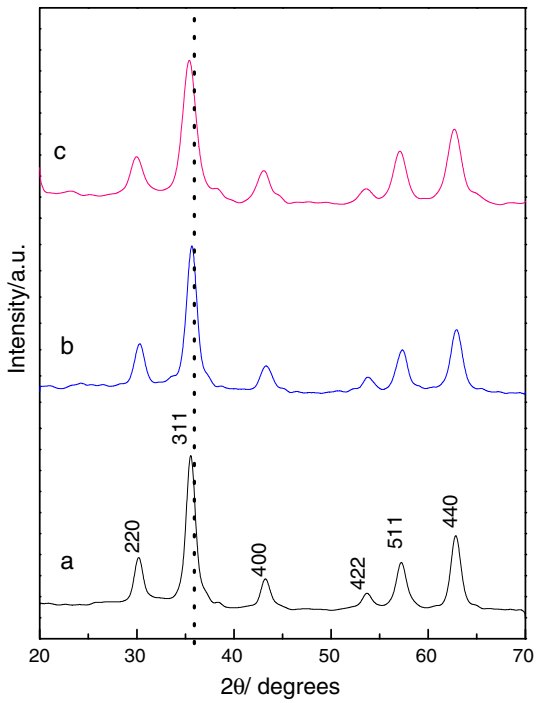

Fig. 1 Powder X-ray diffraction patterns of the MNPs (*a*), CS–MNP (*b*), and BA–CS–MNP (*c*)

Results

X-ray diffraction (XRD)

Powder X-ray diffraction is a non-destructive technique widely used for the characterization of crystalline materials. Various kinds of nano-crystalline materials can be characterized from this technique, including in organics,

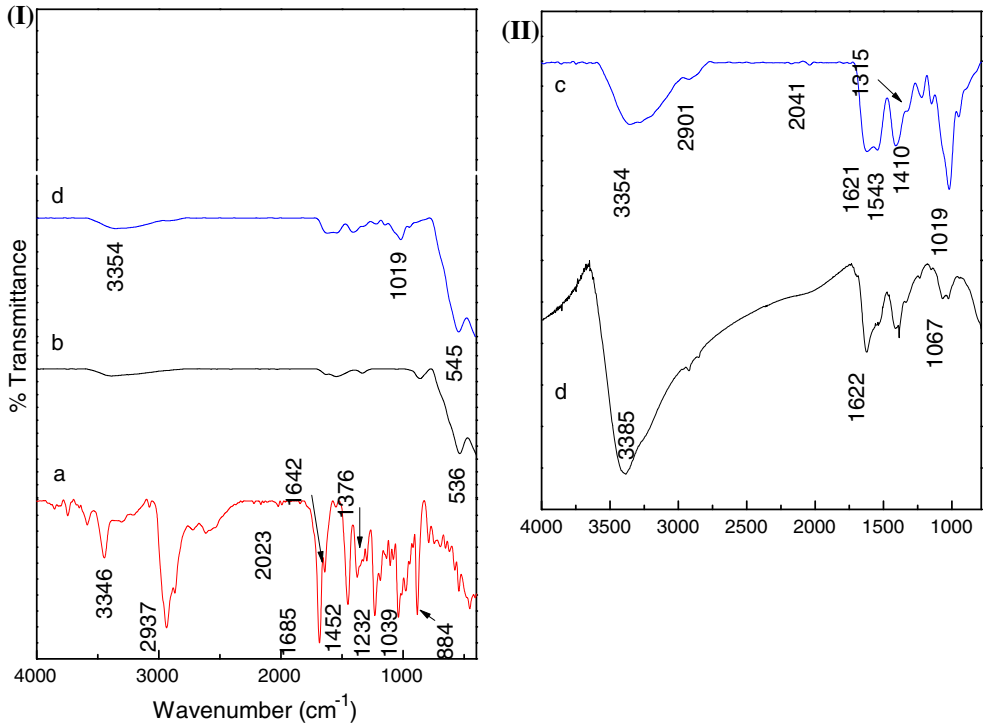

Fig. 2 **I** FTIR spectra of the BA (*a*), MNPs (*b*), and BA–CS–MNP nanocomposite (*c*). **II** FTIR spectra of the BA–CS–MNP nanocomposite (*c*) and CS–MNP nanocomposite (*d*) between 4000 and 785 cm^{-1}

drugs, minerals, zeolites, catalysts, metals, and ceramics. The XRD patterns of the prepared MNPs, CS–MNP, and BA–CS–MNP nanocomposite are shown in Fig. 1a–c, respectively. Figure 1a shows six characteristic peaks that can be indexed as the (220), (311), (400), (422), (511), and (440) [22, 23].

Infrared spectroscopy (FTIR)

The infrared region has main importance for the study of compounds because the IR spectra contain large number of bands and the chance that two compounds have the same infrared spectrum is exceptionally small. Due to this reason, IR spectrum is called the "fingerprint" of a molecule. The FTIR spectra for the free BA, MNPs, and BA–CS–MNP nanocomposite are shown in Fig. 2a–c, respectively. Figure shows the character peak of MNP, BA, and the final product.

Thermogravimetric analysis (TGA)

The thermogravimetric analyzer (TGA) is an important laboratory tool used for material characterization. TGA is used as a technique to characterize nanomaterials used in pharmaceutical and drugs applications. The thermal behavior of the MNPs before and after being coated with CS and loaded with BA was examined using thermogravimetric analysis at Fig. 3.

Measurement of the magnetic properties

A vibrating sample magnetometer (VSM) is a scientific instrument that measures magnetic properties. A nanoparticles sample is placed inside a uniform magnetic field to magnetize the sample. The sample is then physically vibrated sinusoidally, typically through the use of a piezoelectric material. The measurement of the magnetic properties for MNPs and BA–CS–MNP is shown in Fig. 5a, b, respectively.

Transmission electron microscopy (TEM) and zeta potential

The TEM forms an image by accelerating a beam of electrons that pass through the specimen. The electrons are accelerated to 100 keV or higher (up to 1 MeV), projected onto a thin specimen (less than 200 nm) by means of the condenser lens system, and penetrate the sample thickness either un-deflected or deflected. The TEM image of MNPs is shown in Fig. 6a, whereas Fig. 7a–c shows the zeta potential measurement of the free BA, MNPs, and BA–CS–MNP nanocomposite, respectively.

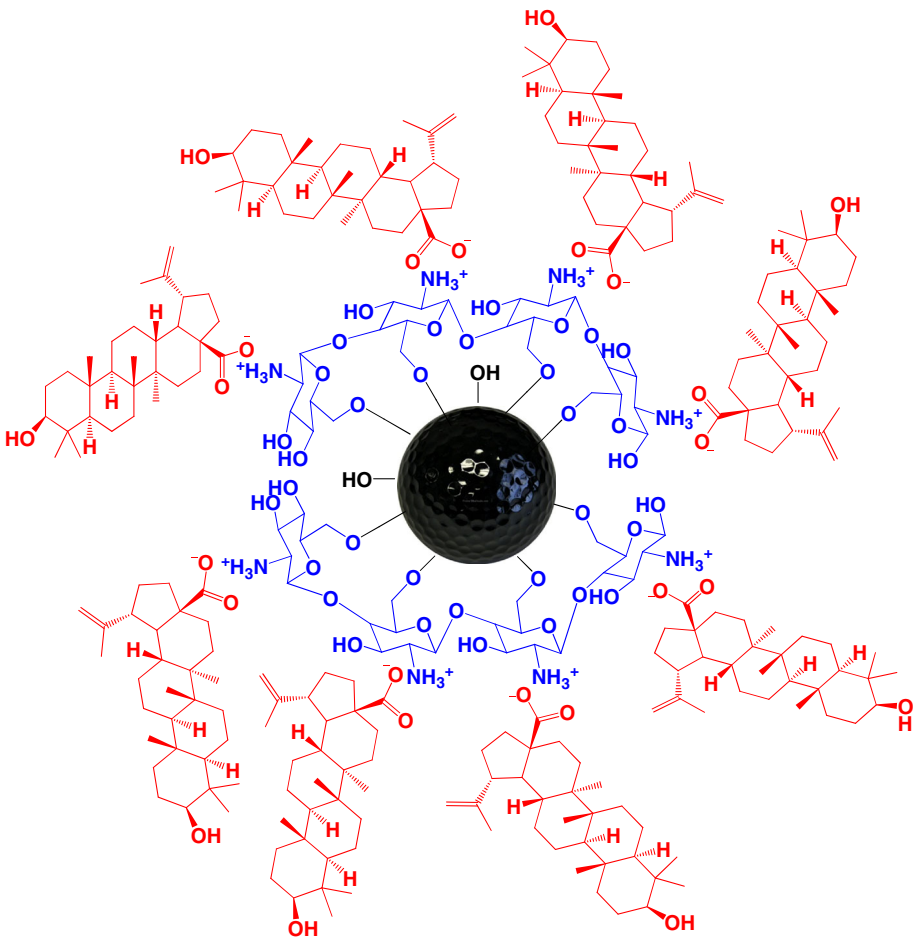

Fig. 3 Schema representing the interactions between the BA, CS, and MNPs in the BA–CS–MNP nanocomposite

In vitro study of BA release from the nanocomposite and kinetic study

The release profiles of BA from the BA–CS–MNP nanocomposite with 6.7 % loading (calculated using UV–Vis) and the physical mixture of BA, CS, and MNPs are shown in Fig. 8. The release kinetic of BA molecules from BA–CS–MNP nanocomposite was described by pseudo-first-order model, pseudo-second-order model, Higuchi model, Hixson–Crowell model, and Korsmeyer–Peppas model.

Cytotoxicity studies

The MTT assay is a colorimetric assay for assessing cell viability. Organism enzymes may, under defined conditions, reflect the number of viable cells present. These enzymes are capable of reducing the tetrazolium dye MTT 3-(4,5-dimethylthiazol-2-yl)-2,5-diphenyltetrazolium bromide to its insoluble formazan, which has a purple color. The cytotoxicity of MNPs, CS–MNP, BA, and BA–CS–MNP nanocomposite on 3T3 and MCF-7 cells was assessed using an MTT assay (Fig. 10).

Discussion

X-ray diffraction (XRD)

The result at Fig. 1 suggests an cubic spinel structure for the magnetite (Fe_3O_4) nanoparticles [24]. The diffraction patterns are also observed for the CS–MNP and the BA–CS–MNP nanocomposites at Fig. 1b, c, respectively.

The average crystallite size was calculated using the Debye–Scherrer formula as shown in Eq. (1):

$$D = \frac{k\lambda}{\beta \cos\theta} \tag{1}$$

where D is the average crystallite size in nm, k is the Scherrer constant which equals 0.9, λ is the diffraction wavelength (0.15418 nm), β is the full width at half maximum intensity that corresponds to the lattice plane (311) at $2\theta = 35.4°$, and θ is the Bragg diffraction angle in degrees. The estimated average crystallite size of MNPs and BA–CS–MNP was calculated to be 39.6 and 23.6 nm, respectively. The size of the BA–CS–MNP nanocomposite decreased, compared to MNPs, due to prolonged and vigorous stirring at a high speed after the addition of the

polymer and the drug [25]. This result can be explained by the energy transfer: When the stirring rate is increased, the energy transferred to the suspension medium is increased, the reaction solution can be dispersed into smaller droplets, and the size is reduced [26].

Infrared spectroscopy (FTIR)

The FTIR spectra of MNPs in Fig. 2b showed two peaks at 3435 and 536 cm^{-1} that might be attributed to an O–H vibration of the adsorbed water and an Fe–O vibration, respectively [15, 27]. The band at 536 cm^{-1} was shifted to 545 cm^{-1} in the BA–CS–MNP nanocomposite (Fig. 2c). These bands (536 and 545 cm^{-1}) confirm the presence of magnetite nanoparticles in these two samples. The absorption bands of free BA are shown in Table 1. In the FTIR spectrum of the BA–CS–MNP nanocomposite, some of the bands disappeared, and the others were shifted due to the nature of the interaction between the chitosan and the BA. For example, the band at 1685 cm^{-1} due to C=O stretching in the carboxylic acid group disappeared, and in addition, two new were formed due to asymmetric and symmetric stretching in COO^-. This result indicates that the BA was loaded on the surface of CS–MNP.

In the FTIR spectrum of the CS–MNP in Fig. 2d, the 1622 cm^{-1} peak is related to the NH_2 group bends of chitosan, and the band for C–N appeared at 1067 cm^{-1}.

Figure 3 provides the schema describing the interactions between the BA, CS, and MNPs. The CS binds the MNPs through glycosidic bonds that appeared in a band at 1076 cm^{-1} in the FTIR spectrum [10]. The COO^- group of BA interacts with the protonated amino group (NH_3^+) from CS, which appeared at 1543 cm^{-1} in the FTIR spectrum [28].

Table 1 Assignment of FTIR absorption bands from BA and BA–CS–MNP nanocomposite

Functional groups	Absorption peak (cm^{-1})	
	BA	BA–CS–MNP
$R_2C=CH_2$	883	880
C–O stretching of alcohol	1039	1019
Symmetrical deformation of $–CH_2$ of a cyclopentane	1452	1410
C=C vibration ($R_2C=CH_2$)	1642	Overlap with COO^-
C=O vibration of carboxylic acid	1685	Disappeared
$–CH_3$ symmetrical vibration (C–H)	2937	2901
OH vibration of an alcohol	3447	3354
Asymmetric and symmetric COO^- stretching	–	1621 and 1315

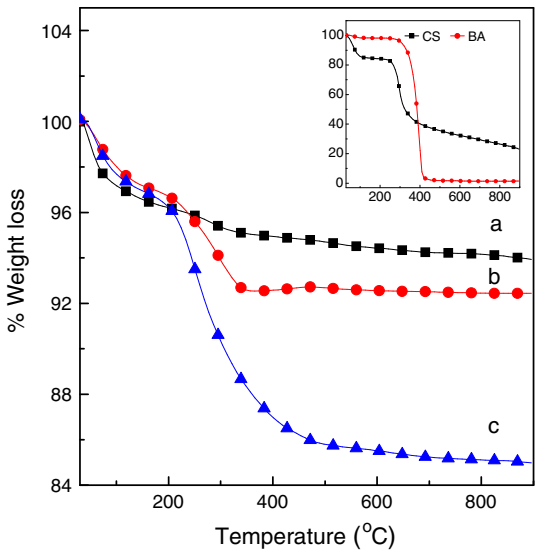

Fig. 4 TGA analysis curves of the MNPs (*a*), CS–MNP (*b*), and BA–CS–MNP (*c*) samples; the inset provides the TGA curve for pure CS and BA

Thermogravimetric analysis (TGA)

The thermal behavior of BA occurred in the region of 353–419 °C and is attributed to the sublimated it with a 98.8 % weight loss [29]. Figure 4a shows that the thermal decomposition of MNPs progressed through one stage of weight loss up to 200 °C. This weight loss occurred due to the removal of surface hydroxyl groups and/or adsorbed water with 5.8 % weight loss [15, 27, 30].

Figure 4b shows that the thermal decomposition of the CS–MNP occurred with a 7.7 % weight loss due to the removal of surface hydroxyl groups and decomposition of the CS at the surface of MNPs. By comparing the weight loss curves for the MNPs and CS–MNP, the quantity of CS on the surface of the MNPs was estimated at 1.9 %. The TGA analysis curve of the BA–CS–MNP nanocomposite is shown in Fig. 4c. The total weight loss from this sample was 14.4 %. This weight loss could be attributed to the removal of surface hydroxyl groups, decomposition of CS, and sublimation of BA.

The percentage of BA loaded onto the BA–CS–MNP nanocomposite was estimated using the UV–visible method. The percentage of BA in the final nanocomposite was 6.7 %. This result is close to the difference in weight loss between the final nanocomposite and the CS–MNP sample.

Measurement of the magnetic properties

The magnetic properties for MNPs and BA–CS–MNP are shown in Fig. 5a, b, respectively. The MNPs and BA–CS–MNP samples prepared in this work had superparamagnetic

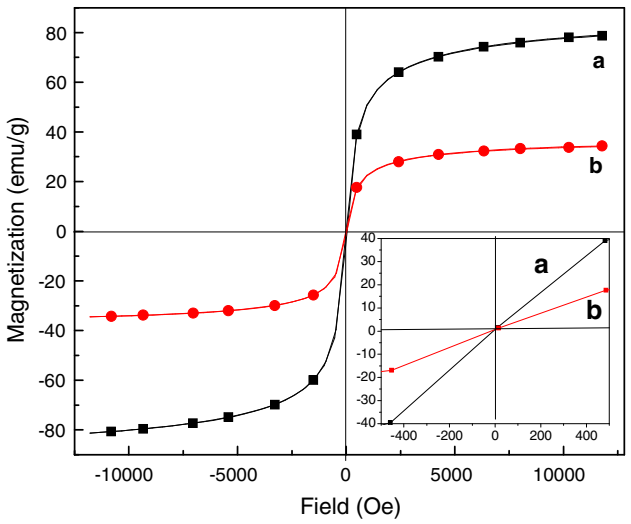

Fig. 5 Magnetization curves of the (*a*) MNPs, and (*b*) BA–CS–MNP recorded at room temperature. The *inset* provides the magnetic behavior under low magnetic fields

properties as verified by the lack of hysteresis in the magnetization curves measured via VSM (inset in Fig. 5). The figure shows a typical magnetization (M) versus the applied magnetic field (O_e) plot at room temperature (300 K). The MNPs sample shows a superparamagnetic property (i.e., no remanence effect) and saturation magnetization of approximately 80.1 emu g^{-1}. As Fig. 5b shows, similar to MNPs, BA–CS–MNP also indicates a zero remanent magnetization, suggesting that superparamagnetic behavior was retained in the nanocomposite. The magnetization value for the nanocomposite was 34.4 emu g^{-1}, and this result was due to the coating of MNPs by the polymer [31].

Transmission electron microscopy (TEM) and zeta potential

The TEM image of MNPs is shown in Fig. 6a, indicating that an average size for the MNPs is approximately 13.0 nm, and the shape of the particles is spherical. The TEM image shown in Fig. 6b discloses that the BA–CS–MNP nanocomposite exhibited mostly a separated and well-dispersed appearance with a spherical shape. The presence of the CS polymer matrix tends to maintain the size of the MNPs and decrease the aggregation process. The BA–CS–MNP diameter was calculated as approximately 13.0 nm.

Figure 7a–c shows the zeta potential measurement of the free BA, MNPs, and BA–CS–MNP nanocomposite, respectively. The zeta potential of free BA is approximately −17.7 mV, whereas the zeta potential of MNPs was −11.4 mV. The zeta potential of the BA–CS–MNP nanocomposite had a positive value compared to MNPs with +25.8 mV value. The positive value of the nanocomposite may facilitate the entry of the BA to cells compared to free BA, which has a high negative charge.

In vitro study of BA release from the nanocomposite

The release profiles of BA from the BA–CS–MNP nanocomposite with 6.7 % loading (calculated using UV–Vis) and the physical mixture of BA, CS, and MNPs are shown in Fig. 8. The BA release from the physical mixture at pH 7.4 was very fast and completed within 23 min. The speed of this release was similar to the literature [8, 32]. The release rate of BA from the nanocomposite is obviously lower than the release rate of BA from the physical mixture, indicating that the anion of BA interacted with the positive charge of CS, which is shown in Fig. 3. In addition, the percent release of BA from the nanocomposite reaches approximately 100 % within approximately 3000 min when exposed to a pH 7.4 environment. This release would occur through a diffusion of the BA drug in the solution of PBS.

Release kinetics of BA from the BA–CS–MNP nanocomposite

The release process of BA molecules from BA–CS–MNP nanocomposite can be described by five kinetics models, described below.

1. The pseudo-first-order kinetic model describes the release from nanocomposites in which the dissolution rate depends on the quantity of drug present in the nanocomposite. The equation may be represented in its linear form as Eq. (2) [33].

$$\ln(q_e - q_t) = \ln q_e - k_1 t \quad (2)$$

in which q_e and q_t are the quantity released at equilibrium and the quantity released at any time (t), respectively, and k_1 is the rate constant of the pseudo-first-order release kinetics. If pseudo-first-order kinetics are applicable, a plot of $\ln(q_e - q_t)$ versus t will be linear, and the k_1 value can be obtained from the slope of the linear plot.

2. The pseudo-second-order kinetic equation may be represented in its linear form as Eq. (3) [34].

$$t/q_t = 1/k_2 q_e^2 + t/q_e \quad (3)$$

in which k_2 is the rate constant of the pseudo-second-order release kinetics. If pseudo-second-order kinetics are applicable, then a plot of t/q_t versus t will be linear, allowing for the computation of k_2.

3. The Higuchi model describes the increased release of the drug from the nanocomposites with increasing the square root of time [35].

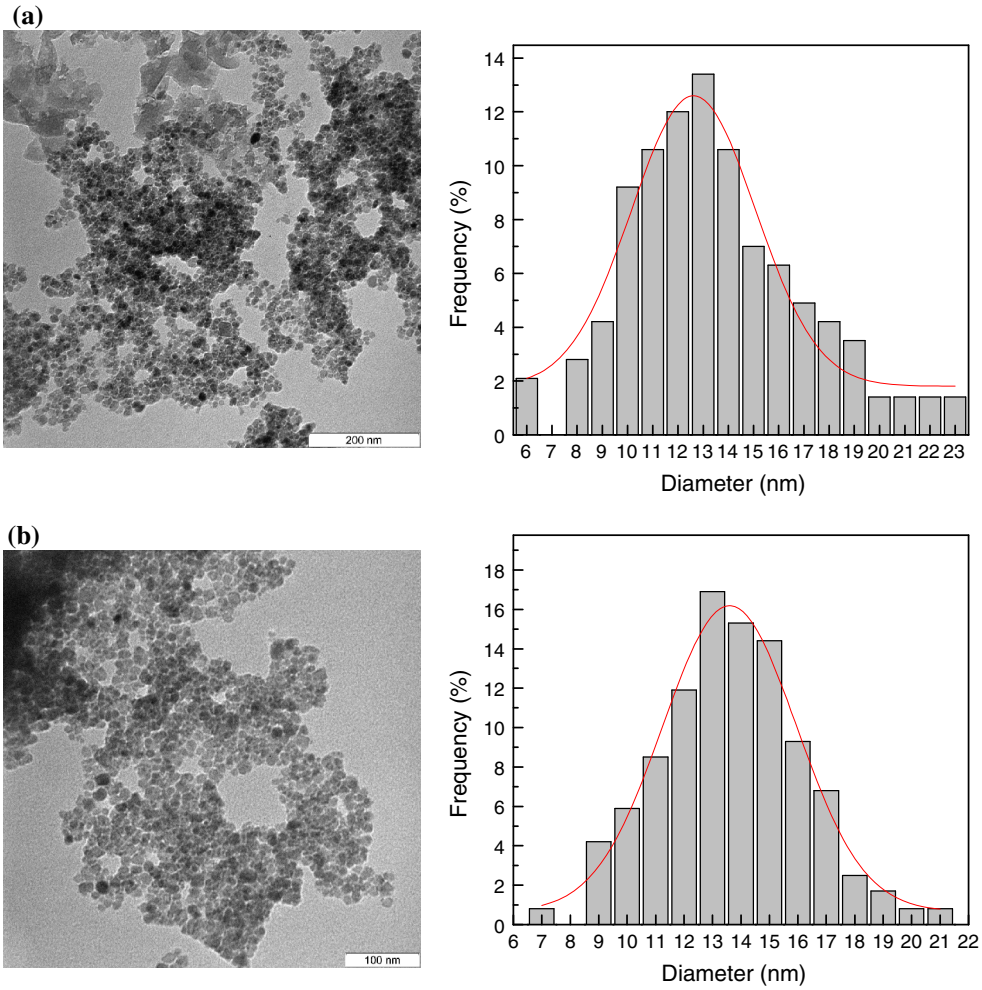

Fig. 6 Transmission electron micrographs for the **a** MNPs and **b** BA–CS–MNP nanocomposite

$$q_t = K_H\sqrt{t} \tag{4}$$

in which k_H is the Higuchi rate constant.

4. The Hixson–Crowell model gives the relationship between the cube root of the percentage of drug remaining in the nanocomposites as a function of time [35].

$$\sqrt[3]{M_o} - \sqrt[3]{q_t} = Kt \tag{5}$$

in which M_o is the initial quantity of drug in the nanocomposite, and q_t is the quantity released at time t.

5. The Korsmeyer–Peppas model gives the relationship between the log of percentage of drug released and the log of time [35].

$$\frac{q_t}{q_\infty} = Kt^n \tag{6}$$

in which q_∞ is the release at infinite time.

With the evaluation of the above five kinetic models for the release kinetic data, the pseudo-second-order model with 0.9916 correlation coefficient (R^2) value was found to be more suitable for describing the release kinetic processes of BA from the BA–CS–MNP nanocomposite (Fig. 9; Table 2).

Cytotoxicity studies

The cytotoxicity of MNPs, CS–MNP, BA, and BA–CS–MNP nanocomposites on 3T3 and MCF-7 cells was assessed using an MTT assay (Fig. 10). In this study, we showed that MNPs and CS–MNP did not show enough cytotoxicity against 3T3 and MCF-7 cell lines. The highest concentration of MNP and CS–MNP (50 μg mL^{-1}) showed 89.8 and 92.1 % viability against the 3T3 cell line, respectively, whereas they showed 73.2 and 87.5 % against the MCF-7 cell line.

The MCF-7 cells were highly sensitive to free BA and BA–CS–MNP compared to 3T3. A deeper look at Fig. 10b makes it clear that the BA–CS–MNP nanocomposites have a higher tumor suppression efficiency compared to BA itself (IC_{50} values for BA and BA–CS–MNP were 3.6 and 2 μg mL^{-1}, respectively). The cell viability of the free BA shows 6.3 %. However, the BA–CS–MNP nanocomposite shows a rapid decrease in cell viability as the concentration increases. The maximum suppression effect of koj–CS–MNP nanocomposites was observed at the concentration of 50 μg mL^{-1}, and this concentration shows 5.9 % in cell viability. The nanocomposite has an advantage because the dose level can be

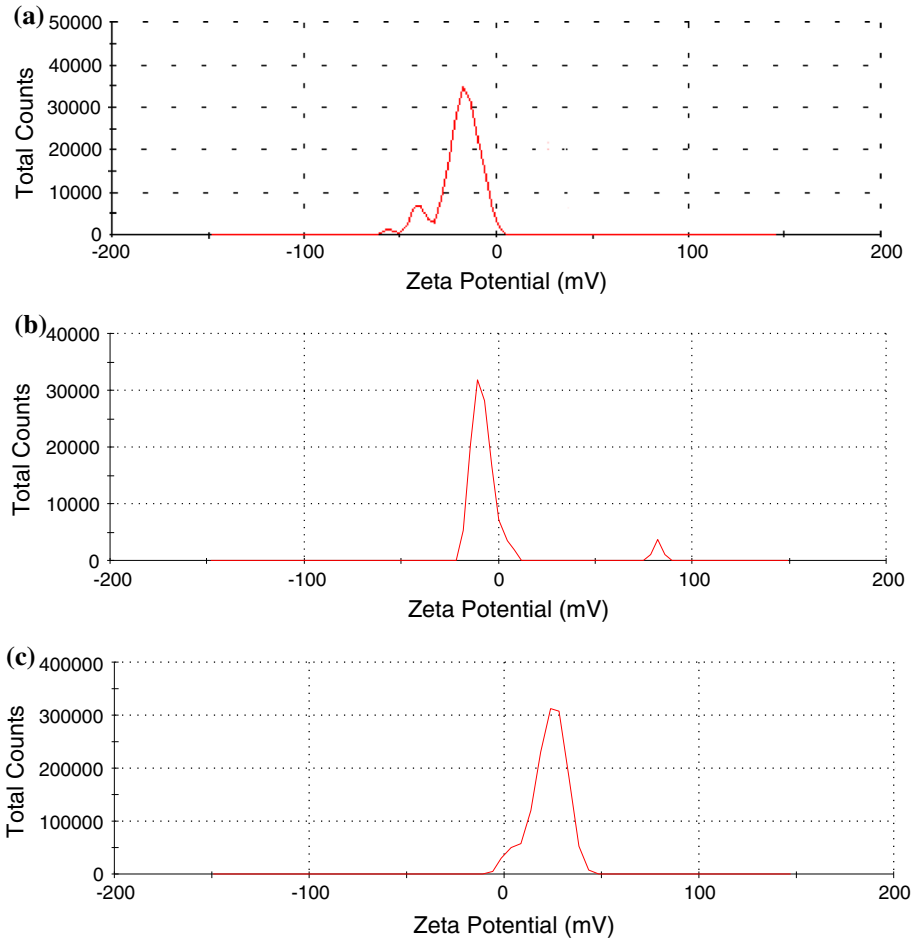

Fig. 7 Zeta potential measurements of free BA (**a**), MNPs (**b**), and BA–CS–MNP nanocomposite (**c**)

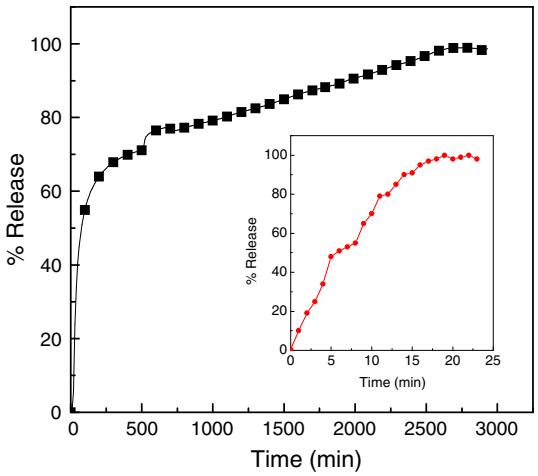

Fig. 8 Release profiles of the BA from the BA–CS–MNP nanocomposite at pH 7.4. *Inset* shows the release profiles of the BA from the physical mixture of BA, CS, and MNPs at pH 7.4

strongly reduced as confirmed by comparing the viability of BA and BA–CS–MNP nanocomposites at 50 μg mL^{-1}. BA–CS–MNP, which contains 3.5 μg mL^{-1} BA (BA loaded in BA–CS–MNP was 7 %), shows 5.9 % cell viability, whereas free BA at approximately 3.125 μg mL^{-1} shows 51.5 % viability. Such a viability gap surely occurs because the BA–CS–MNP nanocomposite could permeate the cell membrane much more effectively than BA itself.

Conclusion

The BA–CS–MNP nanocomposite was prepared by loading the anticancer drug BA on the surface of CS–MNP. The transmission electron microscopy (TEM) of the nanocomposite suggests an average size of 13.0 nm, similar to the pure MNPs nanoparticles. The XRD analysis of the MNPs nanoparticles and the BA–CS–MNP nanocomposite reveals that both contain pure magnetite (Fe_3O_4). The magnetization studies indicate that both the MNPs nanoparticles and the BA–CS–MNP nanocomposite exhibit superparamagnetic behavior. The release of the BA from the nanocomposite followed the pseudo-second-order kinetic model. The BA and BA–CS–MNP nanocomposite exhibit cytotoxicity

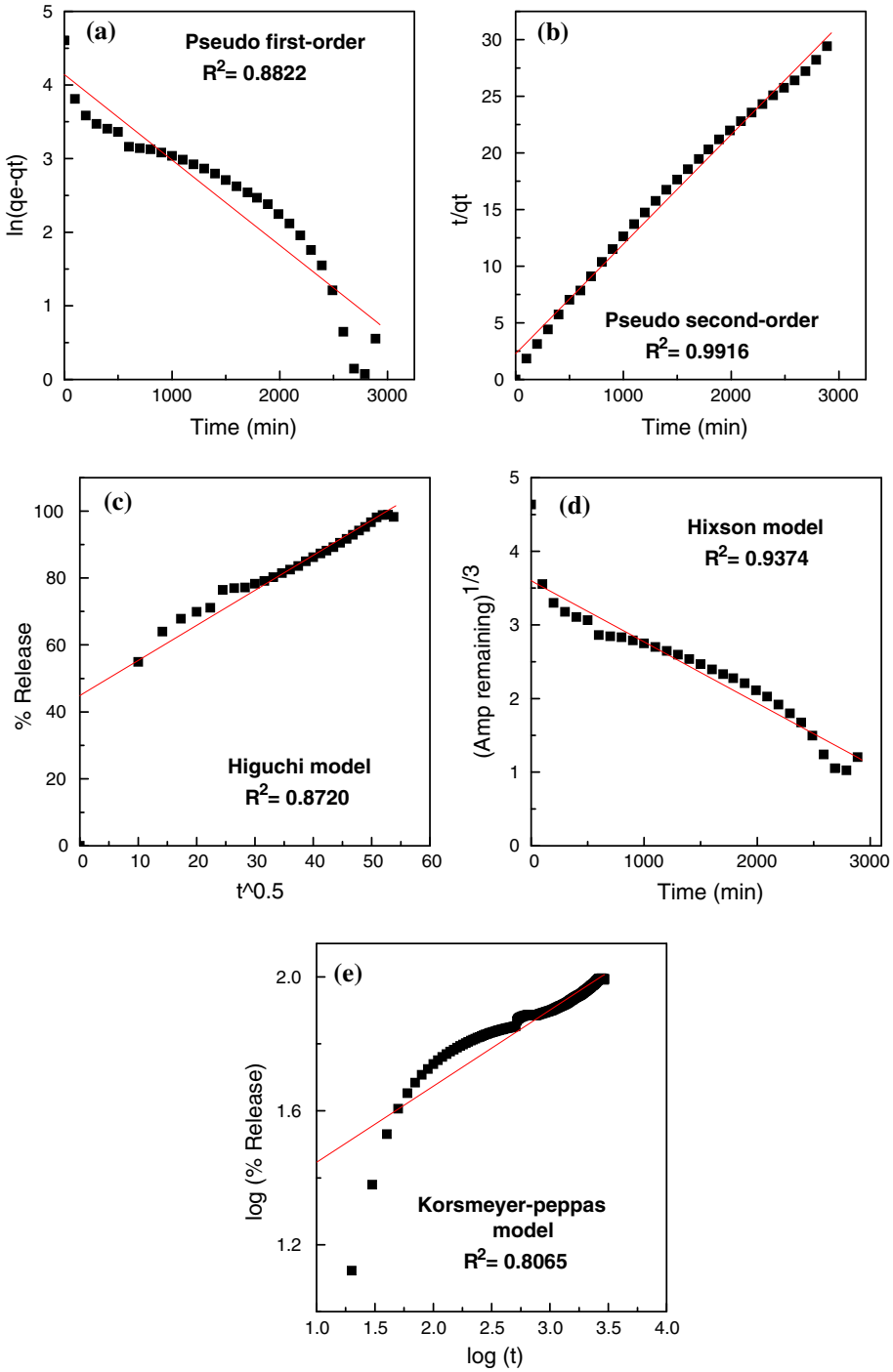

Fig. 9 Data fitting for BA release from BA–CS–MNP nanocomposite using different kinetic models at pH 7.4

Table 2 The correlation coefficients (R^2) obtained by fitting the BA release data from the BA–CS–MNP nanocomposite in PBS solutions at pH 7.4

Samples	Saturation release (%)	R^2				
		Pseudo-first order	Pseudo-second order	Higuchi model	Hixson–Crowell model	Korsmeyer–Peppas model
BA–CS–MNP	100	0.8822	0.9916	0.8720	0.9374	0.8065

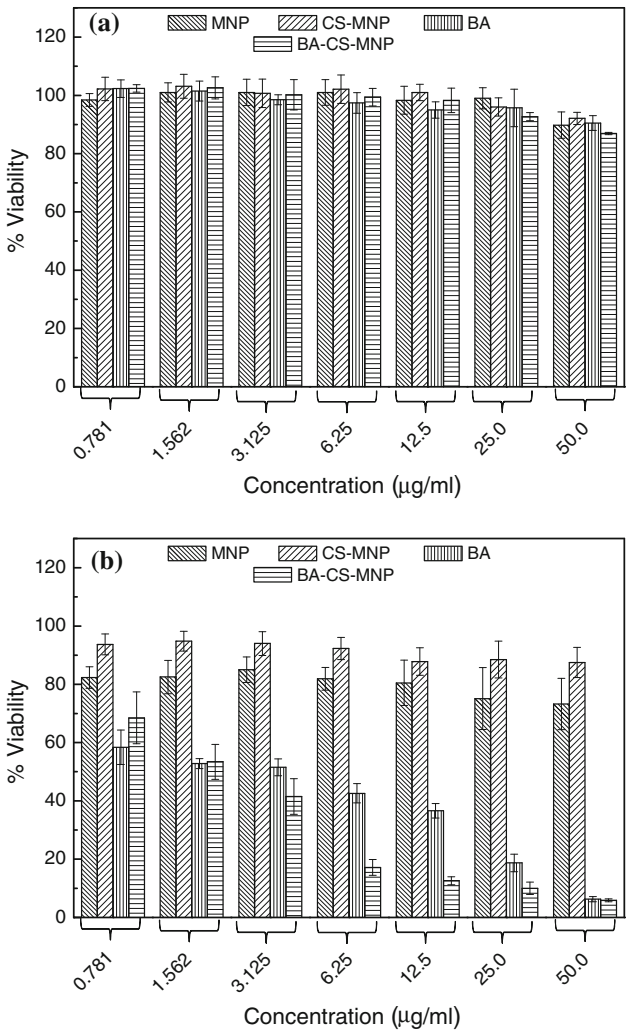

Fig. 10 The cytotoxicity profiles for the MNPs, CS–MNP, BA, and BA–CS–MNP after incubation with 3T3 (**a**) and MCF-7 (**b**) cells as determined via MTT assay. The percentages of viable cells were expressed relative to the control cells ($n = 3$). The results are presented as the mean ± standard deviations

toward MCF-7 cells in a dose-dependent manner with an IC50 value of 2 and 3.6 μg mL^{-1}, respectively.

Acknowledgements The Ministry of Higher Education of Malaysia (MOHE) provided funding for this research under Grant No. 05-03-10-1035 RUGS (vote 9199644).

Conflict of interest The authors report no conflict of interests in this work.

References

1. Pisha E et al (1995) Discovery of betulinic acid as a selective inhibitor of human melanoma that functions by induction of apoptosis. Nat Med 1(10):1046–1051
2. Zuco V et al (2002) Selective cytotoxicity of betulinic acid on tumor cell lines, but not on normal cells. Cancer Lett 175(1):17–25
3. Wick W et al (1999) Betulinic acid-induced apoptosis in glioma cells: a sequential requirement for new protein synthesis, formation of reactive oxygen species, and caspase processing. J Pharmacol Exp Ther 289(3):1306–1312
4. Ji Z-N et al (2002) 23-Hydroxybetulinic acid-mediated apoptosis is accompanied by decreases in bcl-2 expression and telomerase activity in HL-60 cells. Life Sci 72(1):1–9
5. Thurnher D et al (2003) Betulinic acid: a new cytotoxic compound against malignant head and neck cancer cells. Head Neck 25(9):732–740
6. Kim JY et al (2001) Development of C-20 modified betulinic acid derivatives as antitumor agents. Bioorg Med Chem Lett 11(17): 2405–2408
7. Chatterjee P et al (2000) Biotransformation of the antimelanoma agent betulinic acid by *Bacillus megaterium* ATCC 13368. Appl Environ Microbiol 66(9):3850–3855
8. Hussein-Al-Ali SH et al (2014) Arginine–chitosan- and arginine–polyethylene glycol-conjugated superparamagnetic nanoparticles: preparation, cytotoxicity, and controlled-release. J Biomater Appl [Epub ahead of print]
9. Dilnawaz F et al (2010) Dual drug loaded superparamagnetic iron oxide nanoparticles for targeted cancer therapy. Biomaterials 31(13):3694–3706
10. Qu J-B et al (2013) PEG-chitosan-coated iron oxide nanoparticles with high saturated magnetization as carriers of 10-hydroxy-camptothecin: preparation, characterization and cytotoxicity studies. Colloid Surf B 102(1):37–44
11. Wang YX et al (2001) Superparamagnetic iron oxide contrast agents: physicochemical characteristics and applications in MR imaging. Eur Radiol 11(11):2319–2331
12. Mahmoudi M et al (2009) Cell toxicity of superparamagnetic iron oxide nanoparticles. J Colloid Interface Sci 336(2):510–518
13. Xu ZP et al (2006) Inorganic nanoparticles as carriers for efficient cellular delivery. Chem Eng Sci 61(3):1027–1040
14. Chen Y-C et al (2012) In vitro evaluation of the L-peptide modified magnetic lipid nanoparticles as targeted magnetic resonance imaging contrast agent for the nasopharyngeal cancer. J Biomater Appl 28(4):580–594
15. Inbaraj BS et al (2011) The synthesis and characterization of poly (gamma-glutamic acid)-coated magnetite nanoparticles and their effects on antibacterial activity and cytotoxicity. Nanotechnology 22(7):075101
16. Li Z et al (2011) Preparation of magnetic iron oxide nanoparticles for hyperthermia of cancer in a $FeCl_2$–$NaNO_3$–NaOH aqueous system. J Biomater Appl 25(7):643–661
17. Zheng SW et al (2013) RGD-conjugated iron oxide magnetic nanoparticles for magnetic resonance imaging contrast enhancement and hyperthermia. J Biomater Appl 28(7): 1051–1059
18. Panos I et al (2008) New drug delivery systems based on chitosan. Curr Drug Discov Technol 5(4):333–341
19. Unsoy G et al (2012) Synthesis optimization and characterization of chitosan-coated iron oxide nanoparticles produced for biomedical applications. J Nanopart Res 14(11):1–13
20. Predoi D (2007) A study on iron oxide nanoparticles coated with dextrin obtained by coprecipitation. Dig J Nanomater Biostruct 2:169–173
21. Inbaraj BS et al (2012) Synthesis, characterization and antibacterial activity of superparamagnetic nanoparticles modified with glycol chitosan. Sci Technol Adv Mater 13(1):37–44
22. Kumar SR et al (2014) Hydrophilic polymer coated monodispersed Fe_3O_4 nanostructures and their cytotoxicity. Mater Res Express 1(1):015015
23. Kayal S, Ramanujan RV (2010) Anti-cancer drug loaded iron–gold core-shell nanoparticles (FeAu) for magnetic drug targeting. J Nanosci Nanotechnol 10(9):5527–5539

24. Mandal M et al (2005) Magnetite nanoparticles with tunable gold or silver shell. J Colloid Interface Sci 286(1):187–194
25. Li P et al (2004) Synthesis and characterization of a high oil-absorbing magnetic composite material. J Appl Polym Sci 93(2):894–900
26. Sun J et al (2007) Synthesis and characterization of biocompatible Fe_3O_4 nanoparticles. J Biomed Mater Res A 80(2):333–341
27. Kumar R et al (2010) Surface modification of superparamagnetic iron nanoparticles with calcium salt of poly (gamma-glutamic acid) as coating material. Mater Res Bull 45(11):1603–1607
28. Marchessault RH et al (2006) Polysaccharides for drug delivery and pharmaceutical applications. American Chemical Society, Washington, DC
29. Soica CM et al (2012) Physico-chemical comparison of betulinic acid, betulin and birch bark extract and in vitro investigation of their cytotoxic effects towards skin epidermoid carcinoma (A431), breast carcinoma (MCF7) and cervix adenocarcinoma (HeLa) cell lines. Nat Prod Res 26(10):968–974
30. Shan Z et al (2007) Preparation and characterization of carboxyl-group functionalized superparamagnetic nanoparticles and the potential for bio-applications. J Braz Chem Soc 18(7):1329–1335
31. Gupta R, Bajpai AK (2012) Superparamagnetic nanocomposites of poly (vinyl alcohol-*graft*-acrylonitrile) as carrier for magnetically assisted release of ciprofloxacin. Macromol Symp 315(1):73–83
32. Hussein-Al-Ali SH et al (2014) Synthesis, characterization and antimicrobial activity of a novel ampicillin-conjugated magnetic nano-antibiotic. Int J Nanomed 9
33. Dong L et al (2010) Synthesis and release behavior of composites of camptothecin and layered double hydroxide. J Solid State Chem 183(8):1811–1816
34. Ho YS, Ofomaja AE (2006) Pseudo-second-order model for lead ion sorption from aqueous solutions onto palm kernel fiber. J Hazard Mater 129(1–3):137–142
35. Sakore S, Chakraborty B (2013) Formulation and evaluation of enalapril maleate sustained release matrix tablets. Int J Pharm 4(1):21–26